Biophysical and genetic cues regulating the structural remodeling of adipose tissue upon caloric excess

Weinan Zhou
University of Illinois at Urbana Champaign
Sarith Bandara
https://orcid.org/0000-0003-2108-0997
Cecilia Leal (cecilial@illinois.edu)
University of Illinois at Urbana Champaign https://orcid.org/0000-0001-5972-508X
Sayeepriyadarshini Anakk
University of Illinois at Urbana-Champaign

Article

Keywords:

Posted Date: March 14th, 2022

DOI: https://doi.org/10.21203/rs.3.rs-1393426/v1

Abstract

Obesity is an alarmingly common and serious disease. Adipose tissue stores excess calories as triacylglycerol (TAG) and cholesteryl ester in lipid droplets (LDs). How fat packing is regulated in the different adipose depots (white versus brown) and how diet composition alters this packing remain poorly understood. Using small-angle X-ray scattering, we show that LDs are liquid-crystalline, packing TAG in a disordered core with a multilamellar crystalline shell. Western diet increases the number of TAG lamellae in both the depots, while high fat diet alters only the white adipose. Consistently, collagen packs randomly in white fat, forming a permissive environment for LD expansion but is highly oriented in brown fat. During obesity, decrease in chenodeoxycholic acid (CDCA), the endogenous bile acid ligand of Farnesoid X receptor (FXR) is noted. Moreover, FXR deletion leads to enlarged adipocytes, whereas addition of CDCA promotes LD breakdown. These findings uncover that BAs, diet, and tissue niche dictate LD structural remodeling.

Introduction

Obesity is the second leading cause of preventable death in the United States[1]. Adipose tissue routinely expands during obesity to store excess calories within lipid droplets (LDs) in the form of triacylglycerols (TAGs) and cholesteryl esters (CEs)[2]. Rapid and prolonged LD expansion is strongly associated with metabolic diseases. However, the biophysical and genetic mechanisms controlling LD remodeling during abundant nutrition remain elusive.

LDs are typically represented as liquid fat droplets containing disordered TAGs and CEs; yet, how fat structures itself inside the LDs is not fully understood. LDs must efficiently pack fat while nimbly remodeling and expanding in response to metabolic alteration. Therefore, the molecular structural organization in LDs likely contributes to this process. Recently, Shimobayashi and Ohsaki[3] demonstrated that LDs in human hepatocarcinoma cells appear to organize fat in a layered structure at their periphery, and that their organization alters according to the cellular state[4]. Previously, in human osteosarcoma cells[5], a model of layered LDs was postulated where TAGs were surrounded by liquid crystalline (LC) domains of CEs, with the domain size dependent on the TAG:CE ratio. Thus, we anticipated that the LDs of adipocytes (cells of primary fat storage) will remodel their molecular organization to optimize packing, especially in obesity. In this report, we examined fat packing and LD structural properties under normal and obesogenic diets in the different adipose depots.

Bile acids (BAs) are natural detergents of the body known to emulsify fat and form micelles to promote solubilization and absorption[6]. Recently, BA-loaded microparticles were proposed as an alternative to invasive liposuction for the removal of undesired fat deposits[7]. Moreover, the role of BAs as signaling molecules that activate cell surface and nuclear receptors has been well established[8, 9]. Nuclear receptor, Farnesoid X receptor (FXR), a major endogenous BA receptor, is expressed in many tissues[10, 11] and transcriptionally controls lipid metabolism[12, 13]. Previous studies indicated an *in vitro* role for FXR in the

differentiation of white adipocytes[14, 15], and recent work revealed that overexpression of human *Fxr* in mice increased white adipocyte size[16]. We conjecture that BAs will impact LD size, and that the BA-FXR axis may control LD remodeling in adipocytes.

Using X-ray scattering, laser scanning confocal microscopy (LSCM) and a novel adipocyte-specific *Fxr* knockout (Ad-*Fxr*KO) mouse model, we examined how diet, BAs, and FXR affect the biophysical properties of LDs in normal and obese conditions.

Results And Discussion

Deletion of adipose *Fxr* expression results in adipocyte hypertrophy

FXR is expressed in white adipocytes[11] and is known to regulate fat metabolism[12, 13]. We investigated and found detectable levels of *Fxr* transcripts in mature adipocytes isolated from both white adipose tissue (WAT) and brown adipose tissue (BAT) with higher mRNA levels being present in WAT (Supplementary Fig. 1A). To define the role of FXR in adipocytes, we generated Ad-*Fxr*KO mice and confirmed *Fxr* knockdown by qRT-PCR analysis (Supplementary Fig. 1B). We then challenged Ad-*Fxr*KO and f/f *Fxr* mice with either chow, 60% high-fat diet (HFD), or western diet (WD) for 4 weeks. As expected, HFD- and/or WD-fed mice showed increased body weight and fat mass compared to chow-fed mice (Supplementary Fig. 1C, D), which correlated with the increase in transcripts of key lipid synthesis genes *Pparg* and *Dgat2* in WAT (Supplementary Fig. 2B) and BAT (Supplementary Fig. 3B), while SE synthesis genes *Soat1* and *Soat2* were elevated in WAT only after the diet (Supplementary Fig. 2C). The lipolytic gene *Hsl* was decreased in WAT (Supplementary Fig. 2A) but increased in BAT (Supplementary Fig. 3A) upon HFD, indicating an inverse regulation between the two depots. This decrease in WAT *Hsl* expression is not dependent on FXR (Supplementary Fig. 2A). Another lipase, *Atgl* transcript was increased in HFD- and/or WD-fed conditions compared to the normal chow distinctly in BAT (Supplementary Fig. 3A). Despite these gene changes, Ad-*Fxr*KO and f/f *Fxr* mice exhibited similar weight gain and fat mass except for BAT, which weighed higher in WD-fed Ad-*Fxr*KO than WD-fed f/f *Fxr* mice (Supplementary Fig. 1C, D).

We then investigated if there is a difference in individual adipocyte size in the presence and absence of FXR expression. Ad-*Fxr*KO mice showed a notable adipocyte hypertrophy specifically in the white adipose under normal diet (Fig. 1A, B and Supplementary Fig. 4A). When challenged with obesogenic conditions, control animals revealed the expected increase in the size of white and brown adipocytes (Fig. 1A-D and Supplementary Fig. 4A, B). Intriguingly, Ad-*Fxr*KO mice displayed adipocyte hypertrophy in both fat depots compared to the f/f *Fxr* mice (Fig. 1A-D and Supplementary Fig. 4A, B) under HFD and WD. A recent study exhibits a contrasting observation that overexpression of human FXR in mouse adipose tissue enlarges white adipocytes and limits their capacity to expand during obesity[16]. A caveat to the ectopic *Fxr* expression study is that the 3- to 5-fold overexpression is driven by aP2 promoter[16], which can be leaky and induce *Fxr* expression in brain, heart, skeletal muscle, endothelial cells, and adipose-resident macrophages in addition to adipocytes[17, 18], while our findings are based on the analysis of adipocyte-specific *Fxr* knockout (Ad*Fxr*-KO) mice. We also found that Ad-*Fxr*KO mice

exhibited a reduction in the expression of some of the lipogenic and lipolytic genes in white (Supplementary Fig. 2) and brown (Supplementary Fig. 3) fat depots compared to the f/f *Fxr* mice. These findings suggest that adipose FXR may transcriptionally regulate lipid metabolism in adipose tissues.

Diet affects fat packing in an *Fxr*-independent manner

LDs are often treated as amorphous droplets of neutral lipids—predominantly TAGs and CEs—stabilized in the aqueous cytosol by a lipid monolayer and proteins. However, a few recent reports have uncovered that LDs, in cancer or mitotically arrested cell lines, may adopt a liquid crystalline (LC) structure where TAGs and CEs self-organize in layers at an average separation of 3-5 nm[3, 4, 5]. Adipocytes are challenged to store a lot of fat during obesogenic conditions and a LC structure in LDs is a much more efficient way to pack TAGs and CEs than an amorphous configuration.

Synchrotron small-angle X-ray scattering (SAXS) data of both brown and white adipose tissues from Ad-*Fxr*KO and f/f *Fxr* mice fed different diets displayed diffraction peaks at q^{001}= 0.15, q^{002}=0.30, and q^{003}=0.45 Å^{-1}, which are consistent with the presence of a multilamellar liquid crystalline structure with inter-lamellae separation $d^{001}=2\pi/q^{001}$ = 42 Å (Fig. 2A). The multilamellar structure is rather robust persisting to temperatures up to 57 °C (Supplementary Fig. 5). This repeat spacing exceeds by 5 Å of what is expected for CE layers but closely matches the spacing of TAG layers[19] (inset in Fig. 2C). The different possible conformations of TAGs within each layer is depicted in Supplementary Fig. 6[20].

In coexistence with the characteristic multilamellar (*h*,*k*,*l*)=(001), (002), and (003) peaks, there is a broad peak at q = 0.27 Å^{-1} that is consistent with the presence of a disordered fat domain[21, 22, 23, 24]. This is in line with an LD structure where fat packs in a multilamellar LC configuration towards the LD rim and is disordered at the core[4]. How TAGs and CEs partition into the disordered and layered domains is still an open question. CEs and TAGs could phase-separate into either domain[4, 5] or mix at the molecular level and distribute into the disordered and layered regions. A peak at lower q = 0.1 Å^{-1} is one of the diffraction peaks arising from a periodic arrangement of collagen fibers in the tissue extracellular matrix (ECM) which is generally present at q between 0.05 and 0.15 Å^{-1} [25]. While the multilamellar peak position, and hence the spacing between fat layers, appears constant for both adipose tissues and diets, there is a noticeable difference in peak intensity and width. This is important because peak full-width at half maximum *FWHM* directly relates to domain size[26] $\xi = \frac{2\pi}{FWHM \cos\frac{\lambda q}{4\pi}}$ *i.e.* how many layers of fat are packed within a LD (Fig. 2B). For example, WAT LDs have a domain size of 76.4 nm and a layer-to-layer distance of 4.2 nm, which means that there are on average WAT has 10 repeating layers of TAG in chow, 18 in HFD *vs* 23 layers under WD. We find that WD results in LDs with the highest number of fat layers in both WAT and BAT. For instance, the TAG layers in BAT range from 8-11 in chow and HFD but increase up to 16 layers in WD (Fig. 2C). This finding suggests that in response to dietary challenges, LDs remodel not only size, but structure or number of fat layers (Fig. 2C). Excess nutrients from WD and HFD result in

lower CE/TAG ratio and an increase in the domain size, which is consistent with TAG being enriched in the layered domain.

The main difference between HFD and WD is the presence of sucrose in WD. We conjecture that sucrose may facilitate the packing of TAGs in bigger LDs with more packed layers via an osmotic effect. No significant difference in domain size was observed between Ad-*Fxr*KO and f/f *Fxr* genotypes (Fig. 2B).

Polarized optical microscopy (POM) images of LDs isolated from WAT (chow diet) show that the LD rim displays strong birefringence patterns (Fig. 2D) characteristic of smectic liquid-crystalline packing[27, 28]. This is fully consistent with the fact that LDs consist of a disordered liquid-fat core and a shell comprising crystalline fat layers[29]. Remarkably, LDs isolated from WAT under western diet display a very dense rim with strong birefringence (Fig. 2E), fully corroborating the SAXS data that under WD LDs efficiently pack fat by increasing the number of layers at the rim.

Adipose depots display distinct collagen orientation

Remodeling of the ECM is associated with and contributes to adipose expansion[30]. Collagen is the largest group of ECM proteins[31] and often yields a diffraction signal because fibers are bundled at specific and periodic distances from each other[32]. Two-dimensional diffraction patterns of collagen in adipose tissue (Fig. 3A) revealed a stark asymmetric signal for BAT, indicating that the ECM collagen fibers are highly oriented when compared to a symmetric diffraction ring indicating random collagen distribution in WAT. This result is consistent with histology data with collagen stained with picrosirius red (Fig. 3B, C). Collagen has a pericellular deposition in WAT (Fig. 3B) and reticular deposition in BAT (Fig. 3C). Additionally, a more intense collagen peak at q = 0.1 $Å^{-1}$ was observed in the brown compared to white adipose depot (Fig. 2A), supporting that collagen is well oriented and better packed in BAT compared to WAT. Additional experiments are necessary to fully understand the role of collagen morphology in obesity, but we infer that collagen orientation may restrict LD growth and remodeling in an adipose-depot specific manner.

HFD and *Fxr* deletion alter BA composition within adipose tissue

BAs, the natural ligands for FXR[30], are amphipathic molecules[33], and their hydrophilic-hydrophobic ratio determines their capacity to solubilize lipids[33]. Although hydrophobic BAs increase fat solubility, they are known to be cytotoxic[34]. We found that f/f *Fxr* BAT showed higher BA levels and lower hydrophobicity compared to WAT (Supplementary Fig. 7A, B). While Ad-*Fxr*KO mice displayed decreases in β-MCA, the overall hydrophobic index and concentrations remained unaltered compared to f/f *Fxr* mice (Fig. 4A, B and Supplementary Fig. 7A, B). We have previously shown the presence of BAs and the expression of genes responsible for BA synthesis and transport in both fat depots[35], indicating that depot-specific BA transport and/or local synthesis may occur within adipocytes albeit two orders of magnitude lower than in the liver.

HFD-fed f/f *Fxr* mice had different BA composition compared to chow-fed mice in both fat depots (Fig. 4A, B). For instance, primary BAs that are synthesized in the liver—including cholic acid (CA), chenodeoxycholic acid (CDCA), and α muricholic acid (α-MCA)—were decreased, while primary BA β-MCA and secondary BA ω-MCA that are modified by the gut microbiota were increased in the WAT of HFD-fed compared to the chow-fed f/f *Fxr* mice (Fig. 4A). It is interesting to note that adipose tissue has been shown to harbor microbiome that mimics the gut[36, 37] and possibly contributes to the levels of secondary BAs. However, HFD-mediated reduction in CA and increases in β-MCA and ω-MCA were not seen in f/f *Fxr* BAT, suggesting depot-specific alterations to the diet (Fig. 4B). On the other hand, deletion of *Fxr* also leads to alterations in BA composition. Although the ratio of CDCA was lower in the WAT of chow-fed Ad-*Fxr*KO mice, HFD led to a reduction in primary BAs irrespective of the presence or absence of FXR (Fig. 4A). Ad-*Fxr*KO WAT exhibited higher ω-MCA than the f/f *Fxr* mice upon chow, which is reversed under HFD condition (Fig. 4A). In BAT, Ad-*Fxr*KO mice displayed half the amount of β-MCA compared to the f/f *Fxr* mice under chow condition while HFD negated this difference (Fig. 4B). These findings imply that diet and FXR alter primary and secondary BA levels within adipose tissue in a depot specific manner.

BAs break down LDs

HFD enlarged LD size as anticipated and also led to a robust reduction in primary BAs including CDCA levels in adipose tissue (Fig. 4C). CDCA[38, 39, 40] has been shown to reduce TAG levels by inhibiting lipogenic genes[41], inducing fatty acid β-oxidation genes[42], and clearing TAGs in an FXR-dependent manner[43] or promoting energy expenditure via the membrane receptor TGR5[44]. We examined if BAs, besides initiating an intracellular signaling cascade, have a direct role as natural surfactants in regulating LD physical properties in adipose tissue. We isolated LDs and imaged them at different stacked focal planes in the presence and absence of taurochenodeoxycholic acid (TCDCA), the major form of CDCA in mice, using laser scanning confocal microscopy (LSCM). TCDCA at 25 μM or 100 μM—concentrations that are much lower than their critical micellar concentration (CMC) of 3 mM[45]—were sufficient to disintegrate LDs obtained from BAT and WAT into smaller LDs (Fig. 4D). This result suggests that TCDCA can stimulate the breakdown of large LDs and may stabilize small LDs. Combining our data together, we postulate that HFD-induced reduction in TCDCA in adipose tissue may promote LDs with more fat layers during caloric excess (Fig. 2C, D, E). Unmicellized BA surfactants are soluble in the cytosol but tend to adsorb at the LD oil-water interface, reducing its surface tension and facilitating the formation of smaller LDs, which is a putative mechanism underlying LD fission during lipolysis[46].

Overall, our findings reveal that deletion of adipose FXR alters local BA composition and adipose expansion. We show that, beyond size, LDs regulate their structure and fat packing during obesity and that adipose depot-specific collagen orientation may regulate and constrain the extent of adipose tissue expansion. Finally, we demonstrate that BAs in adipose tissue can remodel LD size.

Methods

Animals

Floxed *Fxr* (f/f *Fxr*) mice obtained from Dr. Kristina Schoonjans at Ecole Polytechnique Federale de Lausanne, were bred with mice expressing the Cre-recombinase under the control of adiponectin promoter (Adipoq-Cre, Jackson Laboratory) to generate adipocyte-specific *Fxr* knockout (Ad- *Fxr*KO) mice. Male Ad-*Fxr*KO and f/f *Fxr* mice at 10- to 12-week-old were used. These mice were bred and maintained on a 12:12 light/dark cycle with *ad libitum* access to tap water and a normal chow diet in a climate-controlled (23°C) animal facility at the University of Illinois at Urbana-Champaign. At 10–12 weeks, mice were fed a normal chow (Envigo), 60% high fat (Envigo), or high fat/high sucrose western (Envigo) diet for 4 weeks to mimic obesogenic conditions. Mice were weighed weekly. After 4 weeks, mice were sacrificed at the end of the experimental regimen. Interscapular brown (BAT) and gonadal white (WAT) adipose tissues were collected for isolation of mature adipocytes and analysis of histology, gene expression, fat packing, and bile acid (BA) levels. To examine *Fxr* transcript levels in isolated mature adipocytes and the role of BAs in lipid droplet (LD) structural properties, male C57BL/6 wild-type (WT) mice at 3- to 4-week-old were sacrificed. BAT and WAT were collected for mature adipocytes and LD isolation. All experiments were performed following the National Institutes of Health guidelines for the care and use of laboratory animals, and all procedures were approved by the Institutional Animal Care and Use Committee at the University of Illinois at Urbana-Champaign.

Isolation of mature adipocytes

Mature adipocytes were isolated from Interscapular brown and inguinal white adipose tissue as described previously[47, 48, 49]. Briefly, male C57BL/6 WT mice at 3- to 4-week-old were euthanized by isoflurane inhalational anesthesia followed by cervical dislocation. The interscapular brown and inguinal white adipose depots were harvested and minced with scissors in DMEM (Gibco). Tissue fragments were incubated with digestion buffer ((ddH_2O containing HEPES (100 mM; Fisher Bioreagents), NaCl (123 mM; Fisher Chemical), KCl (5 mM; Fisher Chemical), $CaCl_2$ (1.3 mM; Fisher Chemical), glucose (5 mM; Fisher Chemical), bovine serum albumin (BSA) (1.5% w/v; VWR) and collagenase type I (2 mg/mL; Worthington Biochemical Corporation)), and shaken at 300 rpm at 37°C for 1 hour. The digested solution was then passed through a 100-μm cell strainer and placed on ice for 20 min. The infranatant below the top mature adipocyte layer was removed, and the mature adipocytes were washed with DMEM (Gibco) followed by centrifugation at 200 g for 5 min. Then the top mature adipocyte layer was collected and lysed in TRIzol reagent (Invitrogen) for the following gene expression analysis.

Quantitative real-time PCR

Total RNA was isolated from mature adipocytes and snap-frozen adipose tissues using TRIzol reagent (Invitrogen). Upon DNase I (New England Biolabs) treatment, RNA was reverse transcribed into cDNA using a Maxima reverse transcriptase kit (Thermo Scientific). Quantitative real-time PCR (qRT-PCR) was performed with SYBR green master mix (Applied Biosystems) using Applied Biosystems QuantStudio 7 Flex Real-Time PCR System. To determine relative expression values, the $2^{-\Delta\Delta Ct}$ method was used, where

triplicate Ct values for each sample were averaged and subtracted from those derived from housekeeping gene *36B4*. All primers used are listed in Supplementary Table 1.

Histology

Adipose tissues were fixed in 10% neutral-buffered formalin (VWR) for 24 hours at 4°C and processed. Formalin-fixed tissues were embedded using paraffin and cut on a microtome at 5 µm thickness and mounted onto charged glass microscope slides. Adipose sections were deparaffinized and stained with hematoxylin & eosin (Thermo Scientific) using standard histological protocol. Adipocyte size was quantified using Adiposoft-ImageJ software. Collagen was stained using picrosirius red (Sigma-Aldrich).

Small-angle X-ray scattering (SAXS) of adipose tissue

SAXS experiments were carried out at Beamline 12-ID-B at the Advanced Photon Source at Argonne National Laboratory. An average photon energy of 13.3 keV was used. Tissue samples were either loaded onto a solid sample holder using Kapton tape or centrifuged into quartz capillaries. 2D scattering data were radially averaged using IGOR Pro. The q-calibrant was silver behenate. Data analysis was carried out using Mathematica.

Bile acid analysis

Adipose bile acid (BA) analysis was performed in the NIH West Coast Metabolomics Center at the University of California, Davis. Adipose BAs were extracted from interscapular brown and gonadal white adipose tissue samples (4-4.75 mg) as previously described[50]. Six internal standards (GCA-d4, TCDCA-d4, CA-d6, GCDCA-d4, CDCA-d4, DCA-d4) were added. BA levels were quantified by ultra-high performance liquid chromatography chromatography-triple quadruple mass spectrometry (UHPLC-TQ-MS/MS) (Thermo Fisher Scientific).

Laser scanning confocal microscopy of isolated LDs

LDs were isolated from brown adipose tissue (BAT) and white adipose tissue (WAT) of chow-fed mice based on density gradient centrifugation as described previously[51]. The isolated LDs were incubated with Droplite™ Red staining solution (AAT Bioquest). 50 µL of Droplite™ Red staining solution was added to 100 µL of each of the LD samples, and the samples were incubated at 37°C for 30 minutes. Bile acid TCDCA was then added to the stained LD solution to achieve a final concentration of 1 µM, 25 µM, or 100 µM, and incubated at room temperature for at least 1.5 hours. The samples were then imaged using an LSM800 confocal microscope with a 63x lens at the Leal Lab at UIUC. An excitation wavelength of 561 nm was used for the Droplite™ dye.

Polarized optical microscopy (POM) of isolated LDs

Isolated LDs were imaged using an LSM800 confocal microscope in bright field mode with a fixed polarizer before the camera and a rotatable polarizer after the light source, with the sample placed between the two polarizers on a glass coverslip.

Statistical analysis

Data were expressed as means ± SEM. Statistical analyses were performed using GraphPad Prism 8 software. Differences between two groups were analyzed using Student's *t* test, and multiple group comparisons were analyzed using a two-way or three-way ANOVA with a Fisher's LSD *post hoc* test. $P < 0.05$ was considered statistically significant.

Declarations

Data availability

All data are in the main text and the supplementary information.

Acknowledgments

This work was supported by the Cancer Center at Illinois (FY21, CL and SB), the National Institutes of Health Grant No. 1DP2EB024377-01 (CL and SB), the National Institute of Diabetes and Digestive and Kidney Diseases, R01 DK113080 (SA), USDA HATCH funds ILLU-971-377 (SA), American Cancer Society Grant RSG- 132315 (SA), Cancer center at Illinois (SA) and the Office of Naval Research (ONR) N000141812087 DURIP—Defense University Research Instrumentation Program (LCSM, CL and SB). SAXS experiments were carried out at the beamline 12-ID-B at the Advanced Photon Source (APS), Argonne National Laboratory. Use of APS was supported by the US Department of Energy (DOE), Office of Science, Office of Basic Energy Sciences, under contract number DE-AC02-06CH11357. Adipose tissue BA analysis was performed at the NIH West Coast Metabolomics Center at the University of California, Davis.

Author contributions

W.Z., S.R.B., C.L. and S.A. conceived and designed research; W.Z. and S.R.B. performed experiments and analyzed data; W.Z., S.R.B., C.L. and S.A interpreted data; W.Z. and S.R.B generated figures and drafted the manuscript; all authors were involved in editing and revising the manuscript and had final approval of the submitted and published versions.

Competing interests

The authors have declared that no conflict of interest exis

References

1. Hennekens CH, Andreotti F. Leading Avoidable Cause of Premature Deaths Worldwide: Case for Obesity. The American Journal of Medicine **126**, 97–98 (2013).
2. Cohen P, Spiegelman BM. Cell biology of fat storage. Mol Biol Cell **27**, 2523–2527 (2016).

3. Shimobayashi SF, Ohsaki Y. Universal phase behaviors of intracellular lipid droplets. Proc Natl Acad Sci U S A **116**, 25440–25445 (2019).
4. Mahamid J, *et al.* Liquid-crystalline phase transitions in lipid droplets are related to cellular states and specific organelle association. Proc Natl Acad Sci U S A **116**, 16866–16871 (2019).
5. Czabany T, *et al.* Structural and biochemical properties of lipid particles from the yeast Saccharomyces cerevisiae. J Biol Chem **283**, 17065–17074 (2008).
6. Hofmann AF. Bile Acids: The Good, the Bad, and the Ugly. News Physiol Sci **14**, 24–29 (1999).
7. Safari H, *et al.* Biodegradable, bile salt microparticles for localized fat dissolution. Sci Adv **6**, (2020).
8. Chavez-Talavera O, Tailleux A, Lefebvre P, Staels B. Bile Acid Control of Metabolism and Inflammation in Obesity, Type 2 Diabetes, Dyslipidemia, and Nonalcoholic Fatty Liver Disease. *Gastroenterology* **152**, 1679–1694 e1673 (2017).
9. Li T, Chiang JY. Bile acid signaling in metabolic disease and drug therapy. Pharmacol Rev **66**, 948–983 (2014).
10. Bishop-Bailey D, Walsh DT, Warner TD. Expression and activation of the farnesoid X receptor in the vasculature. Proc Natl Acad Sci U S A **101**, 3668–3673 (2004).
11. Cariou B, *et al.* The farnesoid X receptor modulates adiposity and peripheral insulin sensitivity in mice. J Biol Chem **281**, 11039–11049 (2006).
12. Zhang Y, *et al.* Activation of the nuclear receptor FXR improves hyperglycemia and hyperlipidemia in diabetic mice. Proc Natl Acad Sci U S A **103**, 1006–1011 (2006).
13. Ma K, Saha PK, Chan L, Moore DD. Farnesoid X receptor is essential for normal glucose homeostasis. The Journal of clinical investigation **116**, 1102–1109 (2006).
14. Rizzo G, *et al.* The farnesoid X receptor promotes adipocyte differentiation and regulates adipose cell function in vivo. Mol Pharmacol **70**, 1164–1173 (2006).
15. Abdelkarim M, *et al.* The farnesoid X receptor regulates adipocyte differentiation and function by promoting peroxisome proliferator-activated receptor-gamma and interfering with the Wnt/beta-catenin pathways. J Biol Chem **285**, 36759–36767 (2010).
16. van Zutphen T, *et al.* FXR overexpression alters adipose tissue architecture in mice and limits its storage capacity leading to metabolic derangements. J Lipid Res **60**, 1547–1561 (2019).
17. Lee KY, *et al.* Lessons on conditional gene targeting in mouse adipose tissue. Diabetes **62**, 864–874 (2013).
18. Jeffery E, *et al.* Characterization of Cre recombinase models for the study of adipose tissue. Adipocyte **3**, 206–211 (2014).
19. Tilley AJ, *et al.* Transfer of lipid between triglyceride dispersions and lyotropic liquid crystal nanostructured particles using time-resolved SAXS. Soft Matter **8**, (2012).
20. Takeguchi S, Sato A, Hondoh H, Aoki M, Uehara H, Ueno S. Multiple β Forms of Saturated Monoacid Triacylglycerol Crystals. Molecules **25**, (2020).

21. Yesiltas B, *et al.* Interfacial structure of 70% fish oil-in-water emulsions stabilized with combinations of sodium caseinate and phosphatidylcholine. J Colloid Interface Sci **554**, 183–190 (2019).
22. Conceição ALC, Meehan K, Antoniassi M, Piacenti-Silva M, Poletti ME. The influence of hydration on the architectural rearrangement of normal and neoplastic human breast tissues. Heliyon **5**, (2019).
23. Teubner M, Strey R. Origin of the scattering peak in microemulsions. The Journal of Chemical Physics **87**, 3195–3200 (1987).
24. Kim H, Han M, Bandara SR, Espinosa-Marzal RM, Leal C. Mixing oil and water with ionic liquids: bicontinuous microemulsions under confinement. Soft Matter **15**, 9609–9613 (2019).
25. Conceicao ALC, Meehan K, Antoniassi M, Piacenti-Silva M, Poletti ME. The influence of hydration on the architectural rearrangement of normal and neoplastic human breast tissues. Heliyon **5**, e01219 (2019).
26. Patterson AL. The Scherrer Formula for X-Ray Particle Size Determination. Physical Review **56**, 978–982 (1939).
27. Pelzl G, Hauser A. Birefringence and phase transitions in liquid crystals. Phase Transitions **37**, 33–62 (1991).
28. Bellare JR, Davis HT, Miller WG, Scriven LE. Polarized optical microscopy of anisotropic media: Imaging theory and simulation. Journal of Colloid and Interface Science **136**, 305–326 (1990).
29. Shimobayashi SF, Ohsaki Y. Universal phase behaviors of intracellular lipid droplets. *Proceedings of the National Academy of Sciences* **116**, 25440–25445 (2019).
30. Datta R, Podolsky MJ, Atabai K. Fat fibrosis: friend or foe? JCI Insight **3**, (2018).
31. Chun TH. Peri-adipocyte ECM remodeling in obesity and adipose tissue fibrosis. Adipocyte **1**, 89–95 (2012).
32. Misof K, Rapp G, Fratzl P. A new molecular model for collagen elasticity based on synchrotron X-ray scattering evidence. Biophys J **72**, 1376–1381 (1997).
33. Monte MJ, Marin JJ, Antelo A, Vazquez-Tato J. Bile acids: chemistry, physiology, and pathophysiology. World J Gastroenterol **15**, 804–816 (2009).
34. Hofmann AF, Hagey LR. Key discoveries in bile acid chemistry and biology and their clinical applications: history of the last eight decades. J Lipid Res **55**, 1553–1595 (2014).
35. Zhou W, *et al.*, (2020).
36. Ha CWY, *et al.* Translocation of Viable Gut Microbiota to Mesenteric Adipose Drives Formation of Creeping Fat in Humans. Cell **183**, 666–683 e617 (2020).
37. Massier L, *et al.* Adipose tissue derived bacteria are associated with inflammation in obesity and type 2 diabetes. Gut **69**, 1796–1806 (2020).
38. Angelin B, Einarsson K, Hellstrom K, Leijd B. Effects of cholestyramine and chenodeoxycholic acid on the metabolism of endogenous triglyceride in hyperlipoproteinemia. J Lipid Res **19**, 1017–1024 (1978).

39. Bateson MC, Maclean D, Evans JR, Bouchier IA. Chenodeoxycholic acid therapy for hypertriglyceridaemia in men. Br J Clin Pharmacol **5**, 249–254 (1978).
40. Carulli N, *et al.* Chenodeoxycholic acid and ursodeoxycholic acid effects in endogenous hypertriglyceridemias. A controlled double-blind trial. J Clin Pharmacol **21**, 436–442 (1981).
41. Watanabe M, *et al.* Bile acids lower triglyceride levels via a pathway involving FXR, SHP, and SREBP-1c. The Journal of clinical investigation **113**, 1408–1418 (2004).
42. Pineda Torra I, Claudel T, Duval C, Kosykh V, Fruchart JC, Staels B. Bile acids induce the expression of the human peroxisome proliferator-activated receptor alpha gene via activation of the farnesoid X receptor. Mol Endocrinol **17**, 259–272 (2003).
43. Jiao Y, Lu Y, Li XY. Farnesoid X receptor: a master regulator of hepatic triglyceride and glucose homeostasis. Acta Pharmacol Sin **36**, 44–50 (2015).
44. Chiang JYL, Ferrell JM. Bile acid receptors FXR and TGR5 signaling in fatty liver diseases and therapy. Am J Physiol Gastrointest Liver Physiol **318**, G554-G573 (2020).
45. Pavlović N, *et al.* Bile Acids and Their Derivatives as Potential Modifiers of Drug Release and Pharmacokinetic Profiles. Frontiers in Pharmacology **9**, (2018).
46. Thiam AR, Farese RV, Jr., Walther TC. The biophysics and cell biology of lipid droplets. Nat Rev Mol Cell Biol **14**, 775–786 (2013).
47. Cannon B, Nedergaard J. Cultures of adipose precursor cells from brown adipose tissue and of clonal brown-adipocyte-like cell lines. Methods Mol Biol **155**, 213–224 (2001).
48. Gao W, Kong X, Yang Q. Isolation, Primary Culture, and Differentiation of Preadipocytes from Mouse Brown Adipose Tissue. Methods Mol Biol **1566**, 3–8 (2017).
49. Janke J, Engeli S, Gorzelniak K, Luft FC, Sharma AM. Mature adipocytes inhibit in vitro differentiation of human preadipocytes via angiotensin type 1 receptors. Diabetes **51**, 1699–1707 (2002).
50. La Frano MR, *et al.* Diet-induced obesity and weight loss alter bile acid concentrations and bile acid-sensitive gene expression in insulin target tissues of C57BL/6J mice. Nutr Res **46**, 11–21 (2017).
51. Brasaemle DL, Wolins NE. Isolation of Lipid Droplets from Cells by Density Gradient Centrifugation. Current protocols in cell biology **72**, 3 15 11–13 15 13 (2016).

Figures

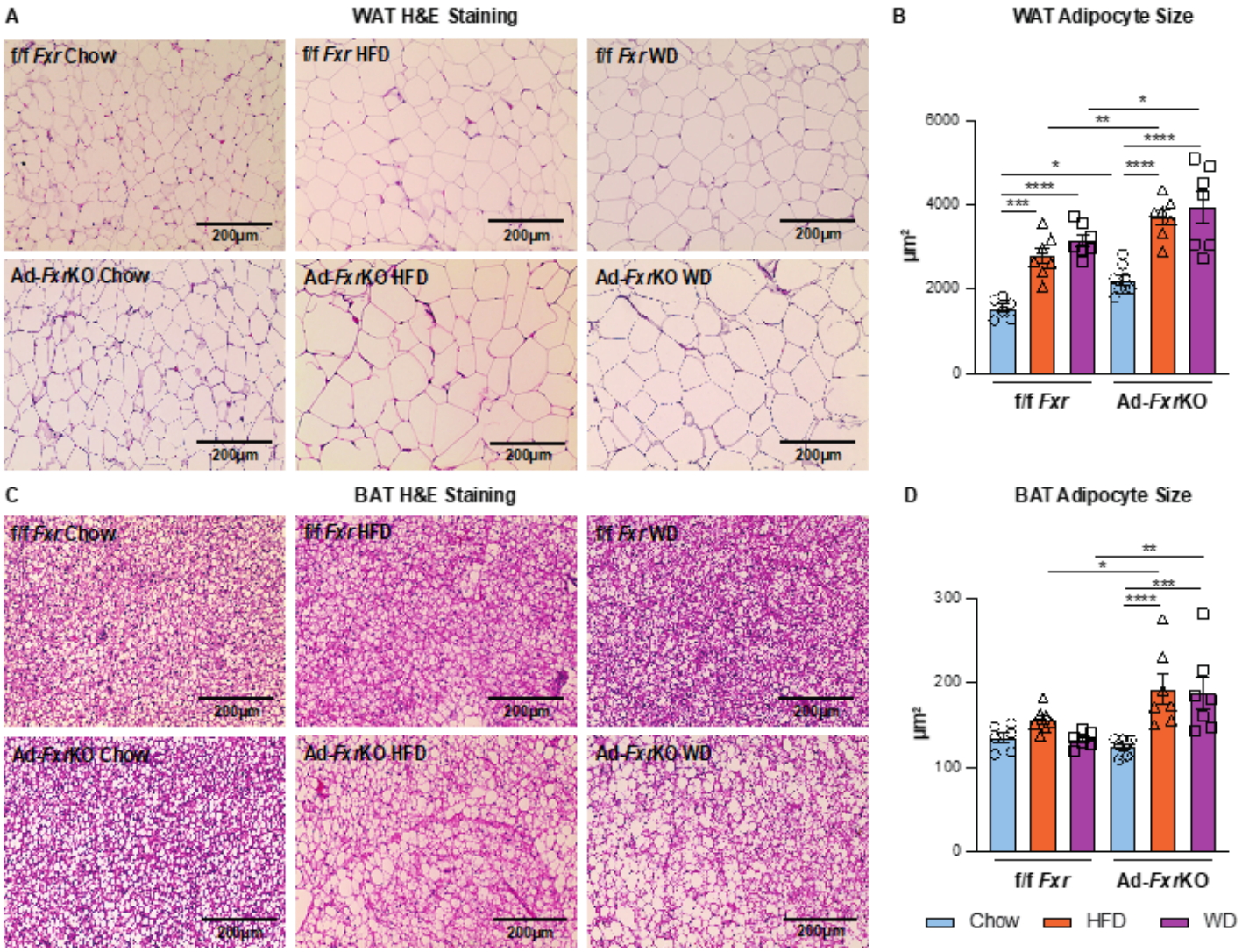

Figure 1

Deletion of *Fxr* results in adipocyte hypertrophy. (A-B) Representative images (A) and the mean (B) of adipocyte size of H&E-stained WAT sections of Ad-*Fxr*KO and f/f *Fxr* mice upon different diets for 4 weeks (n=6-8 mice per group). (C-D) Representative images (C) and the mean (D) of adipocyte size of H&E-stained BAT sections of Ad-*Fxr*KO and f/f *Fxr* mice upon different diets for 4 weeks (n=6-8 mice per group). Data are represented as mean ± SEM. **P* < 0.05, ***P* < 0.01, ****P* < 0.001, *****P* < 0.0001.

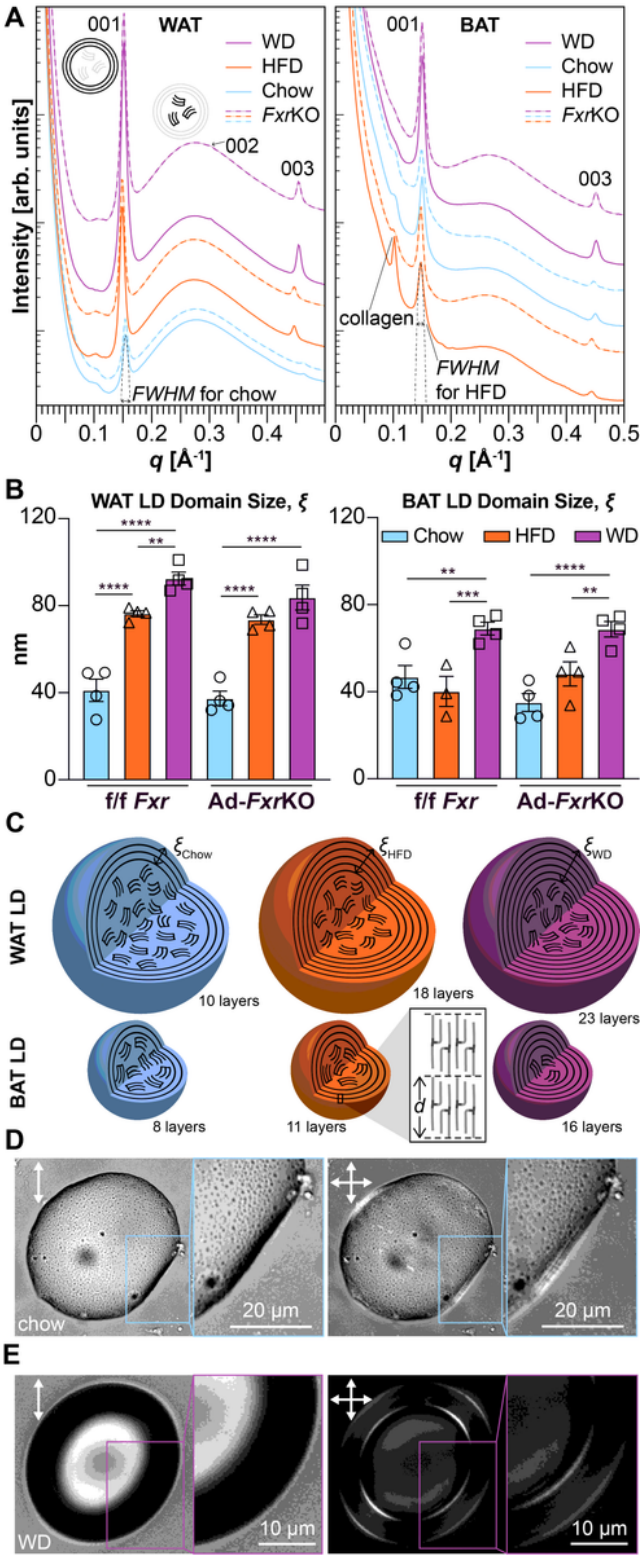

Figure 2

Diet affects fat packing within lipid droplets in adipose tissue in an *Fxr*-independent manner. (A) SAXS data of BAT and WAT from Ad-*Fxr*KO and f/f *Fxr* mice fed different diets display a set of three peaks in the *q range* of 0.15, 0.30, and 0.45 $Å^{-1}$ that arise from (001), (002), (003) diffraction of multilamellar TAG layers in LDs. Multilamellar peaks coexist with a broad peak arising from a disordered domain of TAGs and CEs (n=4 mice per group, 20 locations on tissue per mouse). (B) X-ray data estimation of the size of

the layered domains (in nm) obtained for different depots, diets, and Ad-*Fxr*KO *vs* f/f *Fxr* mice (n=4 mice per group). (C) The number of multilamellar layers in an LD depends on diet. WD yields LDs with the largest number of fat layers. The magnified inset shows how TAG molecules are arranged within the lamellae. Polarized optical microscopy (POM) imaging of isolated LDs from WAT under chow (D) and WD (E). When the polarizers are perpendicular to each other (right), birefringence emerges. This is consistent with an LD rim comprising TAG layers that multiply under WD to pack more fat.

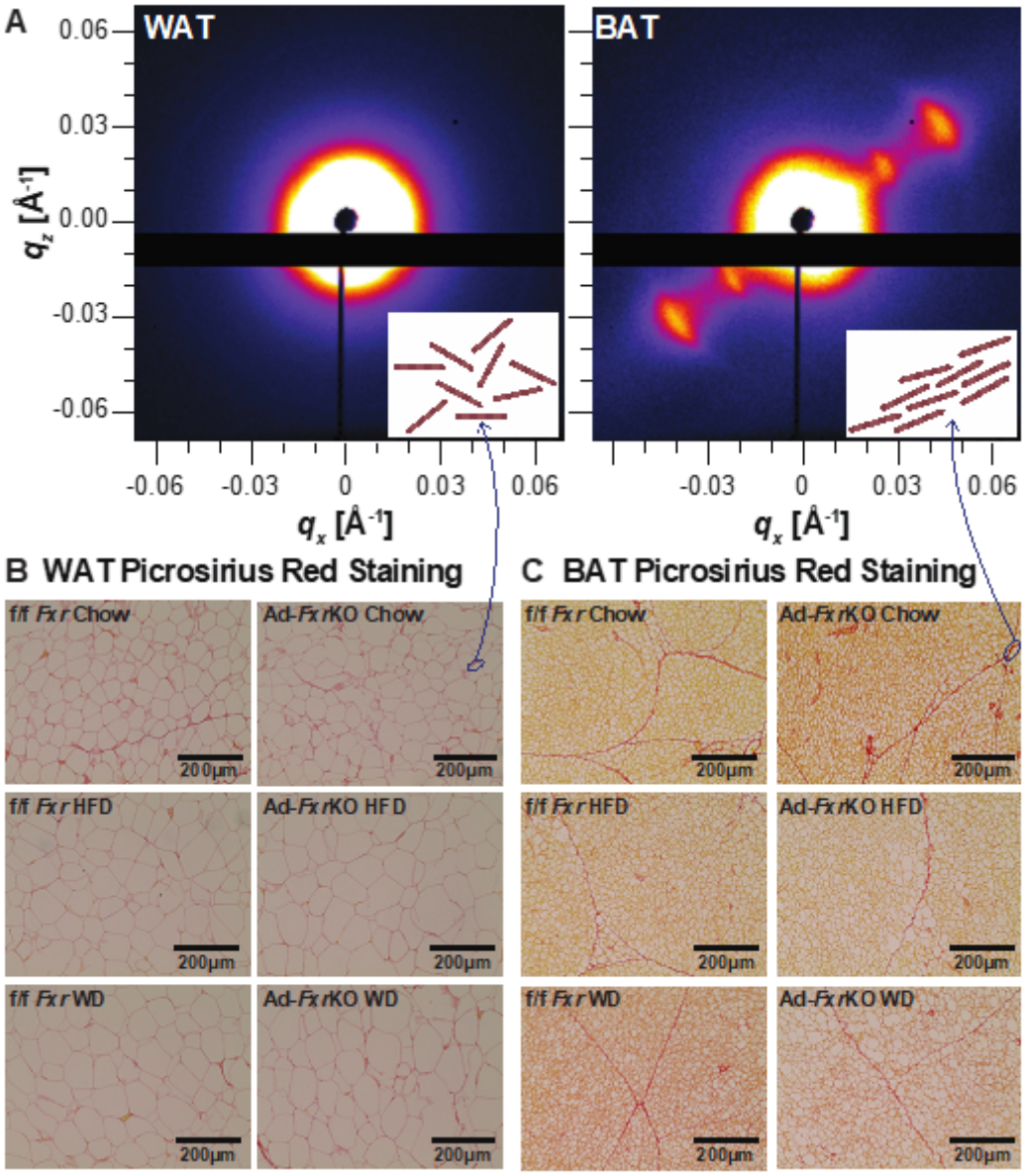

Figure 3

White and brown adipose tissues exhibit distinct collagen orientation. (A) 2D X-ray scattering of BAT and WAT. The inset cartoons represent collagen fibers that are aligned in BAT and randomly oriented in WAT. (B-C) Representative images of picrosirius red-stained WAT (B) and BAT (C) sections of Ad-*Fxr*KO and f/f *Fxr* mice upon chow, HFD, and WD diets for 4 weeks (n=6-8 mice per group).

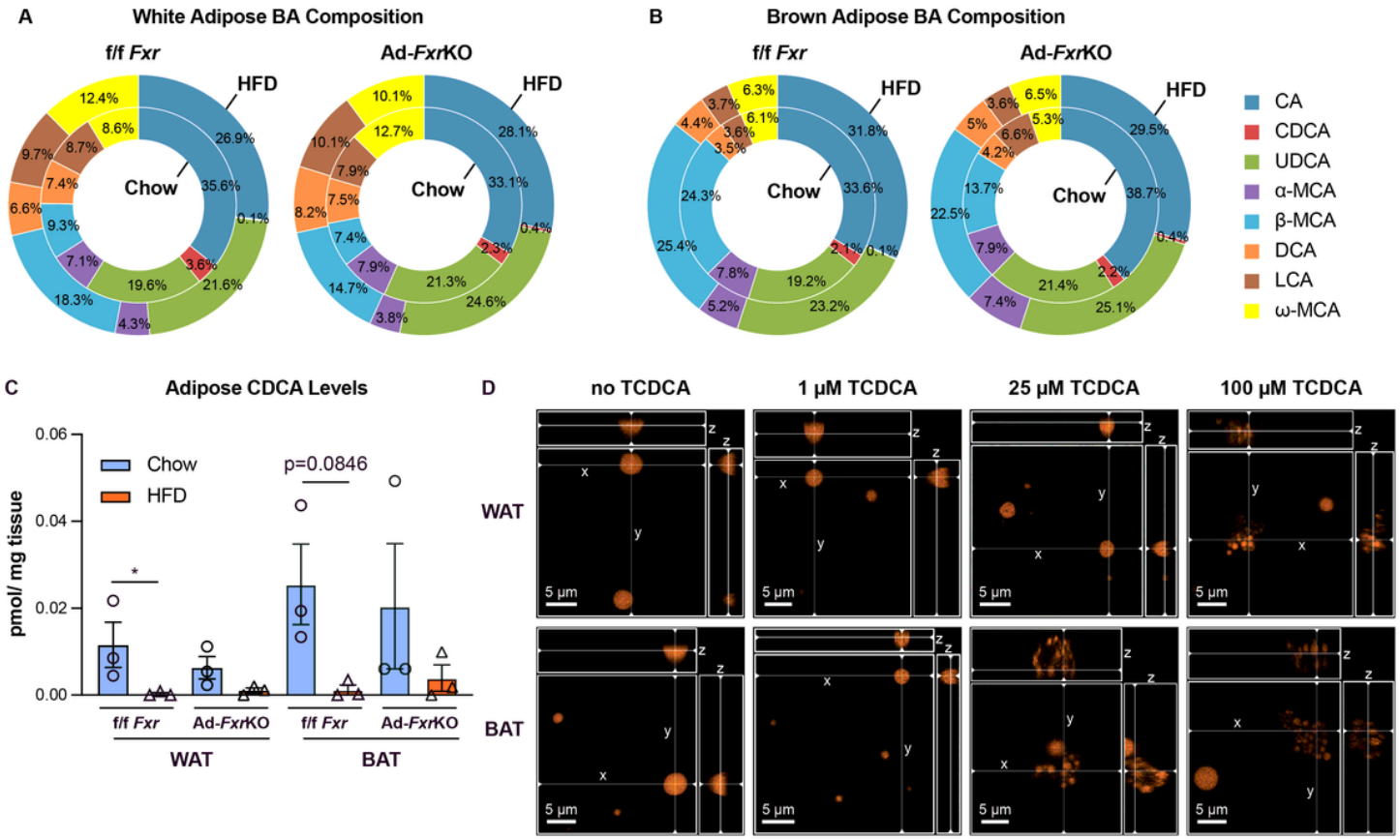

Figure 4

BAs break down lipid droplets, and their composition in the adipose tissue is altered by both HFD and *Fxr* deletion. (A-B) Composition of BAs in the WAT (A) and BAT (B) from Ad-*Fxr*KO and f/f *Fxr* mice upon different diets for 4 weeks (n=3 mice per group). Each BA species includes both free and tauro-conjugated BAs. (C) Levels of TCDCA in the WAT and BAT from Ad-*Fxr*KO and f/f *Fxr* mice upon different diets for 4 weeks (n=3 mice per group). Data are represented as mean ± SEM. **P* < 0.05. (D) 3D Laser scanning confocal microscopy (LSCM) imaging of isolated LDs from WAT and BAT upon TCDCA treatment. Cross-sections of the LDs are shown on the side for a 3D representation.

Supplementary Files

This is a list of supplementary files associated with this preprint. Click to download.

- SupplementaryInformationNatComm021722.docx